Research Article

Adsorption of acid orange 10 on cross-linked porous polyimide

Zengxin Pan[1] · Xin Zhang[1] · Xinbo Wang[1]

Abstract
In this work, a cross-linked porous polyimide (PI) network, fabricated from an "elongated" dianhydride and melamine, was synthesized by polycondensation and thermal dehydration. The as-prepared PI revealed an excellent adsorption performance and removal for acid orange 10 (AO-10) from aqueous solution. The adsorption quantity can reach 599 mg/g when the initial concentration is 500 mg/L with the temperature 298 K and pH value of 3. The maximum desorption ratio can be 38.9%. It is expected that the adsorption quantity and desorption ratio can be optimally improved by changing the length of PI monomer, indicating the cross-linked porous PI network is not only served effectively in sewage treatment but also recycled. *Pseudo-2nd*-order kinetic model and Langmuir isotherm are better fitted with the kinetic data and the adsorption equilibrium data respectively.

Keywords Porous polyimide · Adsorption · Desorption · Acid orange

1 Introduction

Dyes are widely used in fibers, plastics, rubbers, inks, leathers, foods, paper-making, etc. The extensive application of dyes greatly satisfies people's daily life. But it also brings environmental pollution especially industrial wastewaters containing dyes. These industrial wastewaters that contaminated with trace amount of dyes can even cause significant damage to people's health [1]. Therefore, many methods [2–6] have been developed to dispose wastewaters containing dyes. Among these approaches, adsorption is usually adopted as a very simple and effective method.

In the past few decades, porous polymers are often used as adsorbing materials in sewage treatment [7–9]. Among numerous porous polymers, porous polyimide (PI) network has attract much attention because of their excellent mechanical strength, thermal stability and chemical resistance compared with other porous polymers. PI simultaneously contains abundant aromatic components, nitrogen and oxygen atoms in the backbone. In addition, it can be easily functionalized with polar functional groups such as $-NH_2$, $-COOH$, $-CF_3$, $-SO_3H$ and $-OH$ [10–14], which can generate high affinity towards some gas, guest molecules or ions. Therefore, porous PI network is well-suited for adsorbent. Jens Weber et al. [10] fabricated a new microporous polyimide with strong fluorescence based on perylene type dianhydride, which has a high selectivity adsorption for CO_2. Zhonggang Wang et al. [15] synthesized a microporous polyimide network using multi-amino monomer tetraphenyladamantane as crosslinking monomer which exhibited 14.6 wt% uptake of CO_2 at 273 K and 1 bar as well as 1.27 wt% uptake of H_2 at 77 K and 1 bar.

Here, we reported a cross-linked porous PI network using melamine and an "elongated" dianhydride (Scheme 1). In consideration of abundant N atoms in the PI structure, the adsorption/desorption behavior and the adsorption kinetics were discussed in detail to evaluate the adsorption/desorption of the prepared porous PI network for azo dye acid orange 10 (AO-10, Fig. 1).

✉ Xinbo Wang, wangxinboemail@163.com | [1]School of Materials Science and Engineering, Harbin Institute of Technology (Weihai), Weihai 264209, People's Republic of China.

SN Applied Sciences (2019) 1:239 | https://doi.org/10.1007/s42452-019-0243-8

Received: 28 November 2018 / Accepted: 8 February 2019 / Published online: 18 February 2019

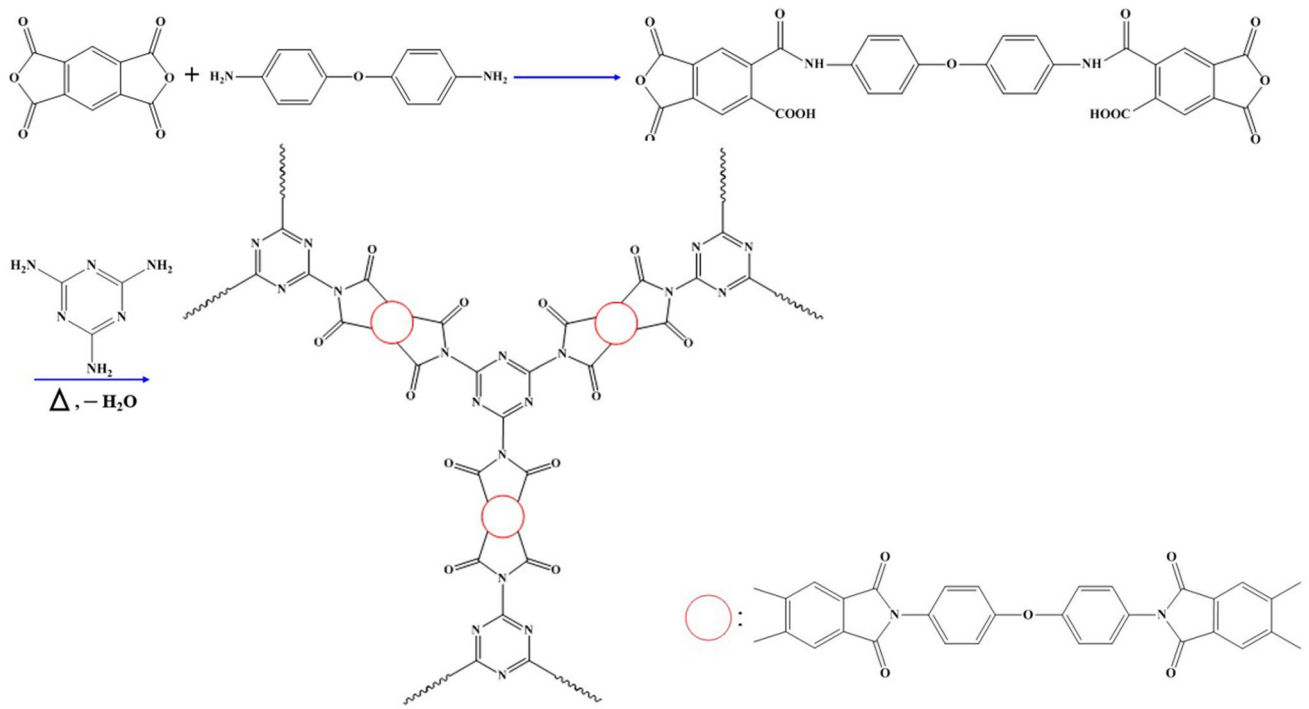

Scheme. 1 Synthesis route of cross-linked porous PI network

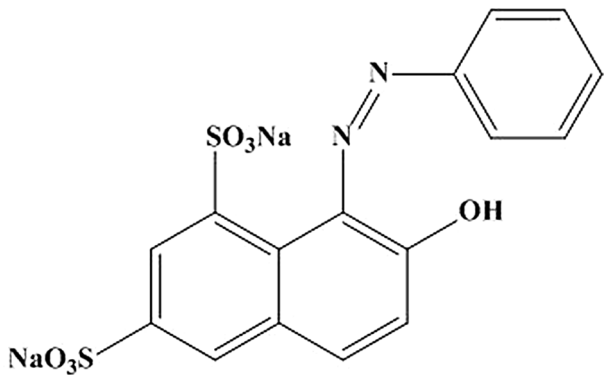

Fig. 1 Chemical structure of AO-10

2 Experimental

2.1 Materials

All reagents were obtained from Sinopharm Cheical Reagent Co., Ltd (Shanghai, China). Melamine (MA) was dried at 120 °C for 4 h under vacuum before use. Pyromellitic dianhydride (PMDA) and 4,4′-oxydianiline (ODA) were purified by sublimation *in vacuo* before use. Dimethylsulfoxide (DMSO, ≥ 99.5%) was dried using molecular sieve. Acetone was used directly.

2.2 Fabrication of cross-linked porous PI network

2.00 g (10 mmol) ODA was dissolved in 42.40 g DMSO at room temperature under stirring; 4.36 g (20 mmol) PMDA was added in small quantities after which the system was stirred continuously for 12 h in ice-water bath with N_2 atmosphere; then 1.26 g MA was added and stirred at room temperature until it was dissolved completely; the reaction system was heated to 180 °C for 24 h with stirring and cooled to room temperature naturally. The yellow solid was collected through filtering and Acetone-washing. Finally, cross-linked porous PI network was obtained after the yellow solid was dried at 120 °C for 4 h under vacuum.

2.3 Characterization

Fourier transform infrared spectroscopy (FTIR) spectra were recorded at a resolution of 1 cm^{-1} with a Nicolet 380 spectrometer. The surface morphologies were recorded by field-emission scanning electron microscopy (FESEM) on a JEOL JSM-6700F using accelerating voltages of 1.5 to 3 keV. The thermogravimetric analysis (TGA) was performed using a TG209F3 instrument thermal analyzer system (Netzsch) at the heating rate of 10 °C/min under N_2 condition with a flow rate of 50 mL/

min. Nitrogen sorption isotherms were conducted on a BET-201A sorptometer from Porous Materials at – 196 °C.

2.4 Adsorption and desorption tests

The synthesized porous PI network was dried in vacuum at 120 °C for 8 h in advance before adsorption test. A series of AO-10 aqueous solutions with different concentration (50 mg/L, 100 mg/L, 200 mg/L, 300 mg/L, 400 mg/L, 500 mg/L) were prepared and the pH values were adjusted to 3 and 7 respectively with hydrochloric acid solution. 2 mg adsorbent (porous PI network) was put in the 10 ml adsorbate solution (AO-10 aqueous solutions) of known concentration at 25 °C and standed for adsorption. The adsorbate solution was separated from adsorbent using 0.22 μL syringe after adsorption with different time. The concentration of separated adsorbate solution was recorded by an UV–Vis detector (wavelength 190–950 nm, Perkin–Elmer). The maximum absorption wavelength of adsorbate was 475 nm. Adsorption equilibrium quantity $q_{a,e}$ was determined by Eq. (1):

$$q_{a,e} = V_a \frac{C_{a,0} - C_{a,e}}{m_a} \quad (1)$$

where V_a (L) is adsorbate solution volume and m_a (mg) is the weight of the adsorbent; $C_{a,0}$ (mg/L) and $C_{a,e}$ (mg/L) were the initial and equilibrium concentration of the adsorbate in solution, respectively.

The desorption test was conducted as following: the adsorbent was collected from adsorbate solution ($C_{a,0}$ = 500 mg/L, pH = 3) when standing for 58 h at 25 °C and dried at 70 °C for 24 h; then 0.7 mg dried adsorbent was added in 5 ml NaOH aqueous solution with the pH value 13 at the temperature 25 °C and standed for desorption. Desorption equilibrium amounts $q_{d,e}$ was determined by Eq. (2):

$$q_{d,e} = V_d \frac{C_{d,e}}{m_d} \quad (2)$$

where V_d (L) is the volume of NaOH aqueous solution with the pH value 13; m_d (mg) is the weight of the dried adsorbent after 58 h adsorption at 25 °C; $C_{d,e}$ (mg/L) were the concentration of released adsorbate from adsorbent in NaOH aqueous solution after completion of desorption.

The depth profiling of adsorbate was determined by confocal Raman microscopy. The chemical composition depth profile of the PI/AO-10 bulk was characterized using a Raman microspectrometer, which combines a Renishaw Raman spectroscope and an inverted Leica DMIRBE microscopy. The laser was used as an excitation source and was focused through a 50× objective to ~ 1 μm light spot on the sample surface. Scattered light from the sample surface was collected through the same objective. Raleigh scattering light was cut off by a holographic notch filter. Raman light was passed through an entrance slit with a 65 μm opening and a 1200 L/mm diffraction grating and then measured by a CCD camera. For the distribution depth profile of the AO-10 within the PI/AO-10 bulk, Raman spectra were acquired from the surface of the focal planes at different depths.

3 Results and discussion

3.1 Characterization of PI

As shown in Fig. 2, the FTIR spectra of PI, AO-10 and PI/AO-10 indicated that the wavenumbers at 1775 cm^{-1}, 1716 cm^{-1}, 1373 cm^{-1} and 721 cm^{-1} were assigned as characteristic peaks of PI. 1175 cm^{-1} and 1034 cm^{-1} were the characteristic peaks of AO-10. After PI had been thoroughly standed in AO-10 solution and dried, the characteristic peaks of both PI and AO-10 appeared (blue curve in Fig. 2), which revealed a successful adsorption of PI to AO-10.

The thermal stability of the prepared PI was investigated with TGA in Fig. 3.

The prepared PI networks exhibited excellent thermal stability with the onset of decomposition at ca. 400 °C ($T_{d,10}$ = 435 °C) under N_2 atmosphere in Fig. 3 as determined by TGA. Small weight losses were observed at the initial stages due to traces of solvent and other volatile substance trapped in the polymer networks. The high thermal stability of prepared PI is ascribed to the plenty of heteroaromatic rings and cross-linking structures in the network in addition to the intrinsic thermal stability of triazine ring from melamine [16].

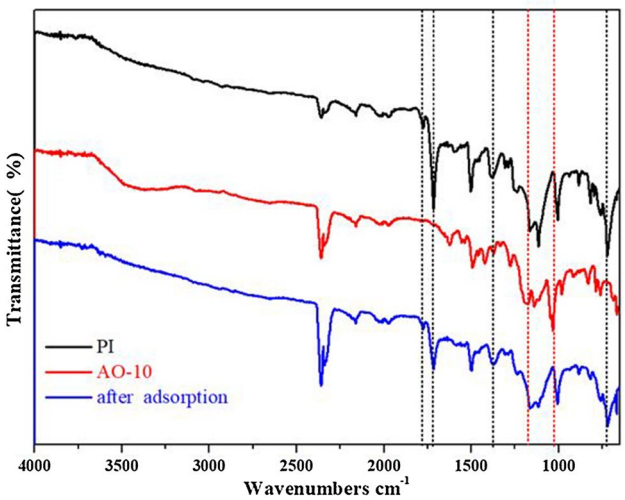

Fig. 2 FTIR spectra of PI, AO-10 and PI/AO-10

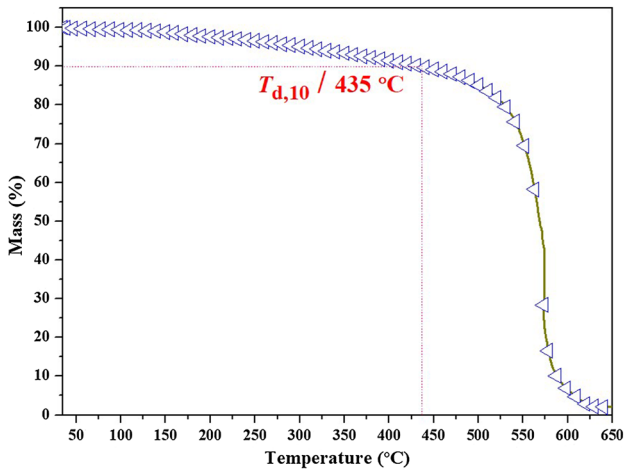

Fig. 3 TGA curve of PI under N_2 atmosphere

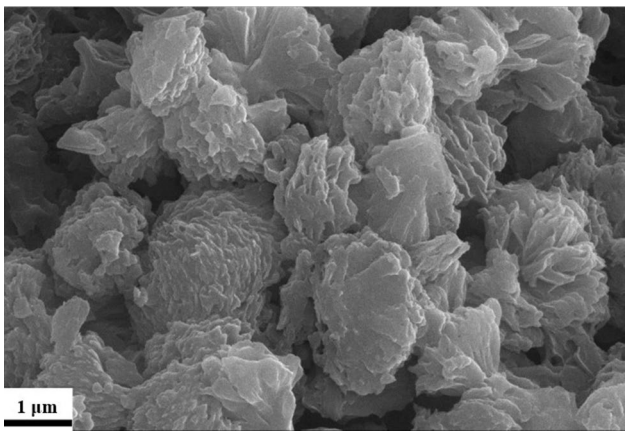

Fig. 4 FESEM image of PI network

From the FESEM image in Fig. 4, there exists highly aggregated clusters with the size 1–2 μm. Obvious petal-shaped patterns can be observed on the surface of every cluster indicating this morphology is beneficial for adsorption.

Figure 5a shows a typical type IV isotherm (BDDT classification, IUPAC) [17]. The initial up-convex part of the Type IV isotherm is attributed to monolayer adsorption during which adsorbent surface has stronger adsorption ability for adsorbate and adsorption quantity increases rapidly. When relative pressure continues to increase, an inflection point appears indicating multilayer adsorption begins. The isotherm shows another convex shape is associated with capillary condensation taking place in mesopores, and the limiting uptake over a range of high P/P_0. The hysteresis loop of Type IV isotherm can be referred to Type H_2 loop, suggesting the existence of randomly distributed nanopores. The isotherm keeps going up at the range of high relative pressure (> 0.9) which implies strong interaction of adsorbent-adsorbate (PI and liquid N_2 in BET test) and continuous multilayer adsorption. The specific surface area by BET is 110.38 m^2/g. The average pore size is 6.7 nm using BJH method from Fig. 5b which is consistent with petal-shaped pattern appeared in the FESEM image of Fig. 4.

3.2 Adsorption kinetics

As shown in Fig. 6, there is an evident pH-dependence adsorption quantity versus time curve. According to the distribution, adsorption quantity of AO-10 decreased sharply when the initial pH value increased from 3 to 7. There are plenty of long pair electrons in PI molecular structure owing to the electron donors (especially O and N atoms). Accordingly, PI surface will be positively charged from the adsorption of electron donors to H^+. Meanwhile, AO-10 will form AO-SO_3^- and Na^+ in water; AO-SO_3^- will approach H^+ captured by electron donors which results in better adsorption of PI to AO-10 under acidic condition [18]. By contrast, adsorption quantity of PI to AO-10 under neutral condition decreased because lower H^+ concentration weakened the interaction between PI surface and AO-10. Therefore, desorption testing can be designed on alkaline condition to evaluate the desorption capability based on the fact. The adsorption quantity increased steadily in both adsorption curves for pH = 3 and pH = 7 until adsorption equilibrium at the time nearly 1500 min. While $q_{a,e}$ value are 377 mg/g and 26 mg/g, respectively.

The *pseudo-1st*-order and *pseudo-2nd*-order kinetic models are introduced in order to evaluate adsorption behavior for $C_{a,0}$ = 200 mg/L and the kinetic parameters are listed in Table 1. The following equations were adopted to express the linear forms of *pseudo-1st*-order and *pseudo-2nd*-order kinetic models:

$$\ln\left(q_{a,e} - q_{a,t}\right) = \ln q_{a,e} - k_1 t \tag{3}$$

$$\frac{t}{q_{a,t}} = \frac{1}{k_2 q_{a,e}^2} + \frac{t}{q_{a,e}} \tag{4}$$

where $q_{a,t}$ is adsorption quantity at time t (min).

As shown in Fig. 7, correlation coefficient (R^2) of *pseudo-1st*-order kinetic curve is lower than that of *pseudo-2nd*-order kinetic curve (0.8618 vs 0.9993, 0.9050 vs 0.9546) which means *pseudo-2nd*-order kinetic model has better correlation than *pseudo-1st*-order kinetic model. It also shows both calculated and experimental values of $q_{a,e}$ are well matched at the condition of pH = 3 (386.1004 mg/g vs 377 mg/g) combined with Table 1. This indicates that both chemical adsorption and physical adsorption exist during adsorption process under the above condition, in the meantime chemical adsorption is possibly the

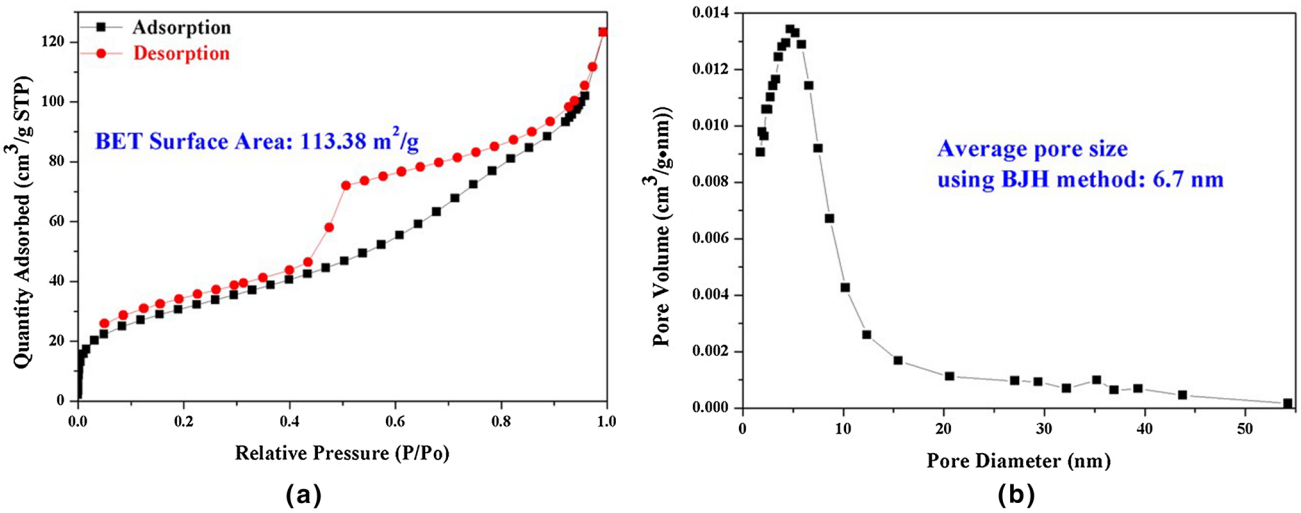

Fig. 5 **a** N_2 adsorption-desorption isotherm obtained at 77 K of prepared porous PI; **b** pore size distribution calculated using the BJH method. The specific surface area around 113.38 m^2/g can be estimated from the BET results. The average pore size distribution can be calculated according to the BJH method with the value 6.7 nm

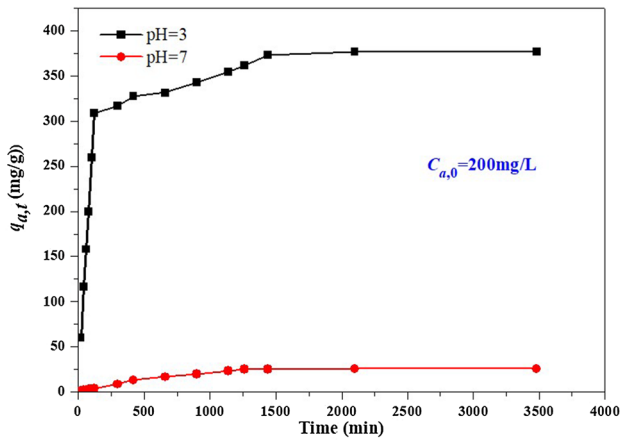

Fig. 6 The relationship between adsorption quantity and time

rate-limiting step and adsorption process is determined by electron sharing or electron exchange [19].

If the movement of dye ions through the bulk liquid to the adsorbent solids is ignored, there are three steps in the adsorption process [20]: firstly, dye ions reach the adsorbent surface through boundary film of liquid–solid (film diffusion); secondly, dye ions arrive specific adsorption activity points via either surface diffusion and/or pore diffusion (intraparticular diffusion); thirdly, the dye ions are adsorbed on the surface of the adsorbent through the active sites. The first or the second step is the rate-determing step while the last step is rapid and assumed to be negligible. To describe the adsorption process of pH = 3, an intraparticular diffusion model developed by Weber and Morriss [21] expressed in Eq. (5):

$$q_{a,t} = k_i t^{0.5} \tag{5}$$

where k_i is rate constant of intraparticular diffusion.

According to this model, plot of $q_{a,t}$~$t^{0.5}$ will be linear from Eq. (5) if the adsorption process is affected by the intraparticular diffusion. It is considered that the intra-particle diffusion is the only rate-controlling step when the line of $q_{a,t}$~$t^{0.5}$ passes through the origin. There are three stages of line segments appeared in Fig. 8 and it indicates that the process of intraparticular diffusion is involved. However, the three lines do not pass through the origin, indicating that some degree of film diffusion control and the intraparticular diffusion is not the only rate-controlling step 20. That the slope of the first line

Table 1 The fitting parameters of *pseudo-1st*-order model and *pseudo-2nd*-order model

PH value	*Pseudo-1st* order			*Pseudo-2nd* order		
	K_1 (/min)	$q_{a,e}^{cal}$ (mg/g)	R^2	k_2 (g/mg min)	$q_{a,e}^{cal}$ (mg/g)	R^2
3	0.00228	190.8714	0.8618	0.00003	386.1004	0.9993
7	0.00258	27.9336	0.9050	0.00005	33.1236	0.9546

$q_{a,e}^{cal}$, calculated value of $q_{a,e}$; k_1, k_2, rate constants of the *pseudo-1st*-order and *pseudo-2nd*-order models, respectively; R^2, correlation coefficient

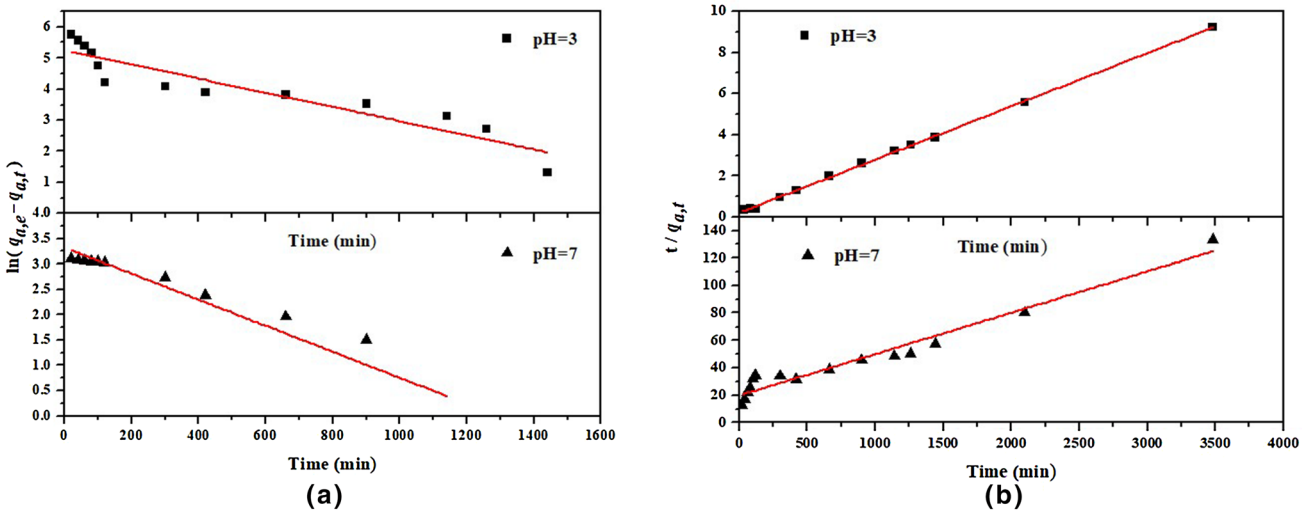

Fig. 7 Kinetic curves of **a**: *pseudo-1st*-order model and **b**: *pseudo-2nd*-order kinetic model with $C_{a,0}$ = 200 mg/g

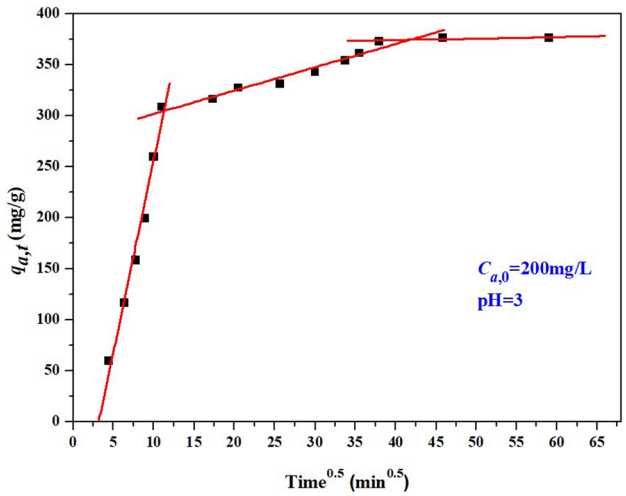

Fig. 8 The internal particle diffusion curve based on Eq. (5)

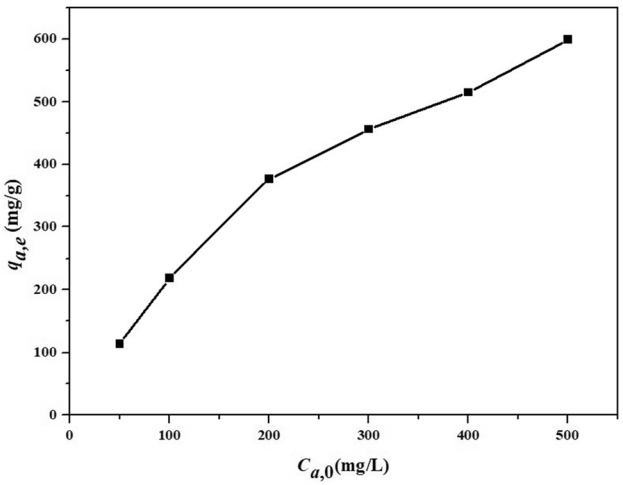

Fig. 9 The effect of initial concentration on the adsorption of AO-10

segment is bigger than that of the second means the first stage is faster than the second stage owing to the film diffusion to some extent. When the concentration of dye ions decreases with the extension of time, the diffusion rate of the film decreases at the same time leading to a decrease in the overall adsorption rate. More importantly, the intraparticle diffusion can be carried out in two stages. The adsorbate molecules rapidly fill the macropores and wider mesopores, and then penetrates the smaller mesopores more slowly [22]. The third line segment refers to the final equilibrium stage in which the intraparticular diffusion slows down and gradually disappears because the dye concentration is very low or has reached the maximum adsorption.

3.3 Concentration effect

It can be seen from Fig. 9 that $q_{a,e}$ increased with the increasing of $C_{a,0}$ under the condition of 298 K and pH = 3. $q_{a,e}$ value reached 599 mg/g when $C_{a,0}$ was 500 mg/L. This means our synthesized porous PI has adsorption or scavenging capability to AO-10. Meanwhile, as the increase of $C_{a,0}$, note that though acid orange dyes have some degree of solubility in water, they will change into aggregations followed by precipitation because of self-association and aggregation among dye molecules when the concentration is too high. However, when the dye concentration is below 0.01 M, the average aggregation is equal to 1 and the risk of aggregation of dye molecules goes away [23]. In our experiments the maximum initial concentration

of AO-10 is 500 mg/L (that is 0.001 M) which implies no aggregation occurs in the concentration range during testing process.

3.4 Adsorption isotherm

Adsorption isotherms of AO-10 on PI with pH = 3 and pH = 7 are plotted in Fig. 10. Langmuir and Freundlich equations [24, 25] are employed to fit the adsorption isotherms shown in Eqs. (6) and (7):

$$q_{a,e} = \frac{Q_{\max} K_L C_{a,e}}{1 + K_L C_{a,e}} \tag{6}$$

$$q_{a,e} = K_F C_{a,e}^{1/n} \tag{7}$$

$$\frac{C_{a,e}}{q_{a,e}} = \frac{C_{a,e}}{Q_{\max}} + \frac{1}{Q_{\max} K_L} \tag{8}$$

$$\ln q_{a,e} = \frac{1}{n} \ln C_{a,e} + \ln K_F \tag{9}$$

where $Q_{\max}$ (mg/g) is maximum adsorption quantity; K_L (L/mg) is Langmuir constant; K_F (mg/g (L/mg)$^{1/n}$) and n are constants in Freundlich model. Equations (8) and (9) are linear form of Eqs. (6) and (7), respectively. The related parameters are summarized in Table 2. It is can be found that the correlation coefficient R^2 of Langmuir model is higher than that of Freundlich model (0.9875 vs 0.9655, 0.9826 vs 0.8455), which demonstrates that the former is more suitable for the adsorption of AO-10 in our experiments and further implies adsorption activity points distribute evenly on porous PI surface. As a result, Q_{max} can be 833.33 mg/g (pH = 3) from Langmuir model. This is more favorable for our prepared porous PI to adsorb AO-10 and the prepared porous PI can eliminate AO-10 in aqueous solution effectively.

Similar adsorption studies have been carried out with azo dyes as adsorbates [26–28]. Table 3 illustrates the capacity of azo dye adsorption using different adsorbents. Obviously organic adsorbents have higher adsorption capacity to azo dyes than inorganic adsorbents. Cross-linked chitosan has higher Q_{max}, but it takes longer time to reach Q_{max} value compared to cross-linked porous PI in this work. During the adsorption test, there is no shaking and only standed in this work while the adsorption process of cross-linked chitosan is shaking all the time; the initial concentration of adsorbate solution in this work is only half of that in the adsorption process of cross-linked chitosan. So to some extent, the cross-linked porous PI exhibits a

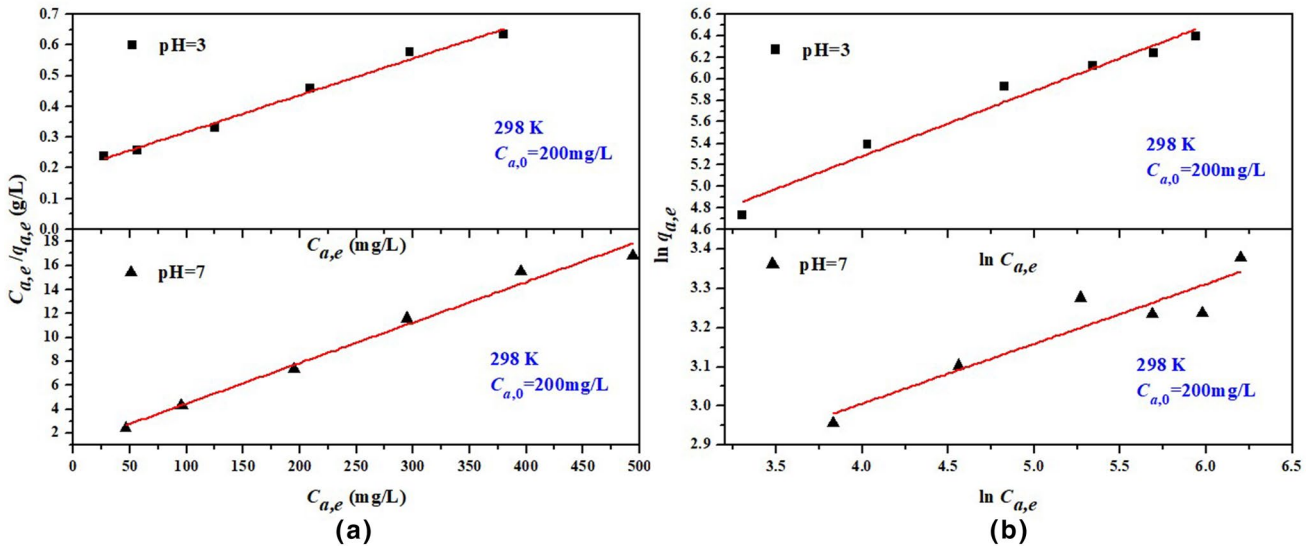

Fig. 10 **a** Langmuir model curve and **b** Freundlich model curve

Table 2 Parameters of AO-10 on porous PI fitted by Langmuir model and Freundlich model

Temperature (K)/pH value	Langmuir model			Freundlich model		
	K_L(L/mg)	$Q_{\max}$ (mg/g)	R^2	n	K_F (mg/g (L/mg)$^{1/n}$)	R^2
298/3	0.0061	833.3333	0.9875	1.6453	17.3072	0.9655
298/7	0.0318	29.4724	0.9826	6.5466	10.9673	0.8455

Table 3 Comparison of maximum adsorption capacity (Q_{max}) of this work and other studies

References	Adsorbent	Adsorbate	pH and temperature (K)	Q_{max} (mg/g)	Time to reach Q_{max} (min)	Initial concentration of adsorbate (mg/L)	Shaking rate (rpm)	Model
This work	Cross-linked porous polyimide (powder)	Acid orange 10	3/298	599	1500	500	0	Langmuir
[26]	Cross-linked quaternary chitosan (powder)	Reactive orange 16	4/298	1060	2000	1000	250	Langmuir
[27]	Modified magnetic silica (powder)	Acid orange 10	3/298	61.33	200	48	400	Langmuir
[28]	Calcined Mg/Al layered double hydroxides	Acid orange 10	4/303	303.1	120	1000	Shaking (the accurate value is not mentioned)	Langmuir

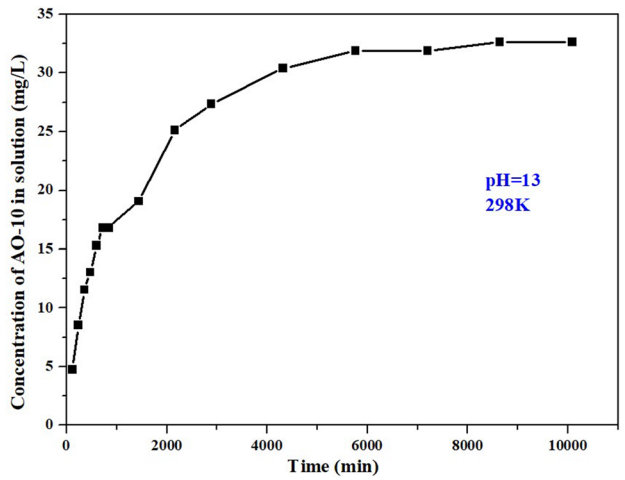

Fig. 11 Concentration–time curve of AO-10 desorption at pH = 13

high-efficiency adsorption capability to azo dyes among organic adsorbents.

3.5 Desorption

When pH value reaches to 13, lots of hydroxide anions gather around PI surface and consequently generates electrostatic repulsion with sulfonate anions. In such situation, the adsorption capability of porous PI to AO-10 decreases inevitably. As is shown in Fig. 11, desorption equilibrium is achieved at the time 120 h. Desorption rate was faster during the first 14 h and 51.5% of AO-10 was desorbed at the time of 14 h. Since $q_{a,e}$ value was 599 mg/g (Fig. 9) in the adsorption testing of $C_{a,0} = 500$ mg/L and $q_{d,e}$ value was 233 mg/g in the desorption testing, it is can be calculated that 38.9% of adsorbed AO-10 was released and 61.1% of adsorbed AO-10 there is still kept in porous PI, which means once AO-10 is adsorbed into porous PI it is difficult to release. We speculate that maybe this is attributed to nano-size effect. Similar phenomenon was found in other research where liquid small molecule compound cannot be released even under reduced pressure after it was adsorbed into the nanochannels of porous matrix [29]. Thus, we believed 38.9% of the released AO-10 is more probably to lie in the very shallow surface area.

We used Raman spectra to examine the dependence of bulk samples at different depths from the surface. In Fig. 12, the wavenumbers at solid lines and dash lines can be marked as the characteristic peaks of PI and AO-10 respectively. We can conclude that no AO-10 is adsorbed at the depth of adsorbent lower than 20 μm from Fig. 12a; while in the desorption testing no signals of AO-10 were found at the surface and the depth of adsorbent lower than 20 μm (Fig. 12b). This strongly confirms that AO-10 is adsorbed by PI in the depth range of 0–20 μm from PI surface and only a small amount of AO-10 in depth range of 0–5 μm from PI surface is released during the desorption process, indicating most AO-10 is kept in the depth range of 5–20 μm. There must exist competition repulsion and attraction between AO-10 and PI during desorption process.

As is mentioned above, all concentrations of AO-10 are lower than the aggregation concentration and thus AO-10 appears as a single stretchable molecule in aqueous solution used in this article. Since AO-10 is still a small molecule, the size of a single AO-10 molecule is not greater than 1 nm. AO-10 can easily enter the channel of the synthesized porous PI (average pore diameter is 6.7 nm from Fig. 5b). So electrostatic interaction became the only factor to determine the adsorption/desorption of AO-10 when porous PI is used. During the adsorption process of pH = 3, electrostatic interaction is favorable to

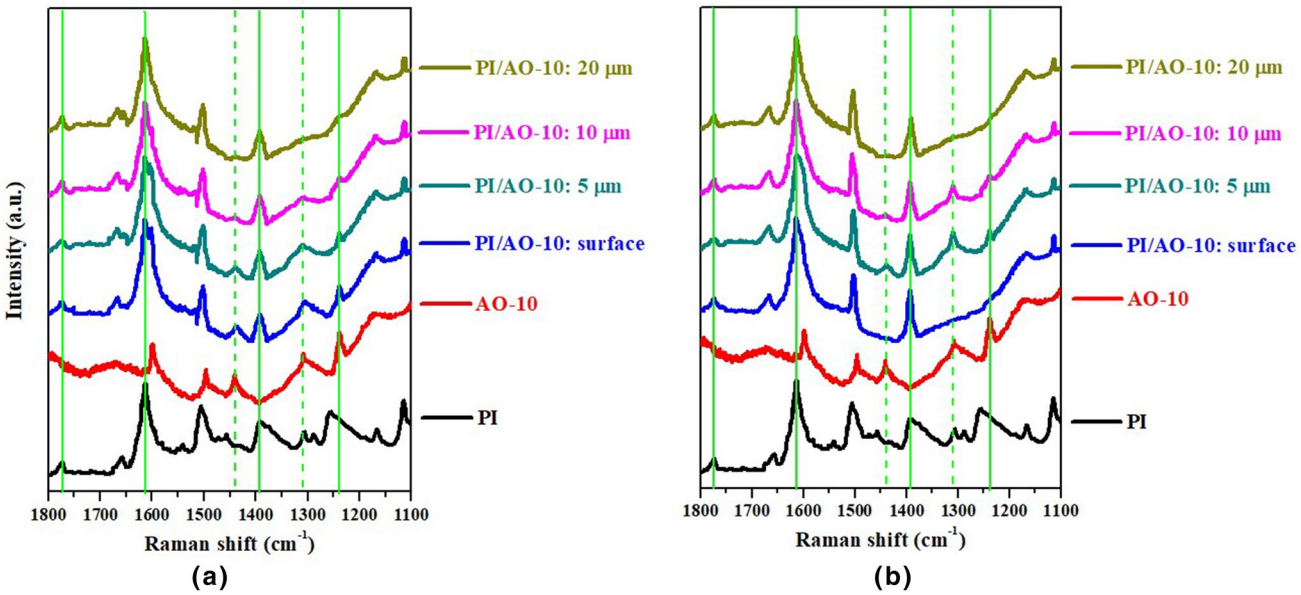

Fig. 12 Raman spectra taken with a focal plane of bulk samples at different depths from the surface of **a**: adsorption testing and **b** desorption testing

adsorption. As more AO-10 molecules are adsorbed in the channels of porous PI, a certain degree of pore-blocking appears unavoidably. It is this reason that no AO-10 molecules were adsorbed at the depth lower than 20 μm. The smaller of the pores, the easier to block the pore channels for adsorbate. Hence, it is believed that the adsorbed layer will become thinner if the pore size decreases. Note that for our porous PI, the pore size can be fine-tuned by regulating the length of dianhydride as demonstrated in Scheme 1. Correspondingly, during the desorption process, different pore size will also affect thickness of the desorbed layer (0–5 μm for the desorption testing in our work) and further desorption efficiency. The relationship between the length of dianhydride and adsorption/desorption is very critical, and the related work is underway.

4 Conclusions

A cross-linked porous PI network was fabricated by an "elongated" dianhydride and used as an efficient adsorbent for the adsorption of AO-10. The prepared PI displayed good thermal stability, abundant micro/mesopores with average pore size 6.7 nm. The adsorption equilibrium quantity can reach 377 mg/g under the condition of 298 K, pH = 3 and $C_{a,0}$ = 200 mg/L within 1500 min. The maximum desorption ratio can be 38.9% under the condition of 298 K, pH = 13 after adsorption equilibrium of $C_{a,0}$ = 500 mg/L. *Pseudo-2nd*-order kinetic model is better fitted with the kinetic data. The Langmuir isotherm correlated better with the adsorption equilibrium data and the maximum adsorption capacity to AO-10 is 833.33 mg/g at 298 K. Meanwhile, changing the length of PI monomer can fine-tune the pore size of synthesized porous PI, suggesting a potential approach to better improve the adsorption of AO-10 by porous PI.

Acknowledgements The authors are very grateful for the assistance in all characterization and testing from the Analysis and Testing Center of School of Materials Science and Engineering, Harbin Institute of Technology (Weihai).

Compliance with ethical standards

Conflict of interest The authors declare that they have no conflict of interest.

References

1. Ahmad T (2009) Oil palm biomass-based adsorbents for the removal of water pollutants-a review. J Hazard Mater 167:1–9
2. Shi BY et al (2007) Removal of direct dyes by coagulation: the performance of preformed polymeric aluminum species. J Hazard Mater 143:567–574
3. Chen W, Lu W, Yao Y, Xu MH (2007) Highly efficient decomposition of organic dyes by aqueous-fiber phase transfer and in situ catalytic oxidation using fiber-supported cobalt phthalocyanine. Environ Sci Technol 41:6240–6245
4. Mahanta D, Madras G, Radhakrishnan S, Patil S (2009) Adsorption and desorption kinetics of anionic dyes on doped polyaniline. J Phys Chem B 113:2293–2299

5. Mahanta D, Madras G, Radhakrishnan S, Patil S (2008) Adsorption of sulfonated dyes by polyaniline emeraldine salt and its kinetics. J Phys Chem B 112:10153–10157
6. Alqadami A et al (2016) Adsorptive removal of toxic dye using Fe_3O_4–TSC nanocomposite: equilibrium, kinetic, and thermodynamic studies. J Chem Eng Data 61:3806–3813
7. Zhang YL et al (2009) Superhydrophobic nanoporous polymers as efficient adsorbents for organic compounds. Nano Today 4:135–142
8. Zou ZM, Jiang CH (2017) Solvothermal polycondensation of novolacs phenolic-resin to nanopowders and their derived activated nanocarbons as efficient adsorbents for water cleaning. J Porous Mater 24:1555–1564
9. Hori K, Sano M, Suzuki M, Hanabusa K (2018) Preparation of porous polymer materials using water-in-oil gel emulsions as templates. Polym Int 67:909–916
10. Liao YZ, Weber J, Faul CFJ (2015) Fluorescent microporous polyimides based on perylene and triazine for highly CO_2-selective carbon materials. Macromolecules 48:2064–2073
11. Kim J et al (2016) One-step synthesis of nano-porous monolithic polyimide aerogel. Microporous Mesoporous Mat 234:35–42
12. Wang Y et al (2016) Porous polyimide framework: a novel versatile adsorbent for highly efficient removals of azo dye and antibiotic. React Funct Polym 103:9–16
13. Einsla BR et al (2004) Sulfonated naphthalene dianhydride based polyimide copolymers for proton-exchange-membrane fuel cells. I. Monomer and copolymer synthesis. J Polym Sci Polym Chem 42:862–874
14. Jin XZ, Ishii H (2005) Novel positive-type photosensitive polyimide with low dielectric constant. J Appl Polym Sci 98:15–21
15. Shen C, Bao Y, Wang Z (2013) Tetraphenyladamantane-based microporous polyimide for adsorption of carbon dioxide, hydrogen, organic and water vapors. Chem Commun 49:3321–3323
16. Wu F et al (2018) Controlled synthesis and evaluation of cyanate ester/epoxy copolymer system for high temperature molding compounds. J Polym Sci Polym Chem 56:1337–1345
17. Sing KSW et al (1985) Reporting physisorption data for gas solid systems with special reference to the determination of surface-area and porosity (recommendations 1984). Pure Appl Chem 57:603–619
18. Yang S, Wu Y, Wu Y, Zhu L (2015) Optimizing decolorization of acid fuchsin and Acid Orange II solution by MnO_2 loaded MCM-41. J Taiwan Inst Chem Eng 50:205–214
19. Ho YS, Mckay G (1999) Pseudo-second order model for sorption processes. Process Biochem 34:451–465
20. Aksu Z, Tatli AI, Tunç O (2008) A comparative adsorption/biosorption study of Acid Blue 161: effect of temperature on equilibrium and kinetic parameters. Chem Eng J 142:23–39
21. Weber WJ, Morris JC (1963) Kinetics of adsorption on carbon from solution. J Sanit Eng Div 89:31–60
22. Lorenc-Grabowska E, Gryglewicz G (2007) Adsorption characteristics of Congo Red on coal-based mesoporous activated carbon. Dyes Pigments 74:34–40
23. Bracko S, Span J (1997) Osmotic coefficients of CI Acid Orange 7 in aqueous solution and in the presence of simple electrolyte. Dyes Pigment 35:165–169
24. Haghseresht F, Lu GQ (1998) Adsorption characteristics of phenolic compounds onto coal-reject-derived adsorbents. Energy Fuel 12:1100–1107
25. Tan IAW, Hameed BH, Ahmad AL (2007) Equilibrium and kinetic studies on basic dye adsorption by oil palm fibre activated carbon. Chem Eng J 127:111–119
26. Rosa S et al (2008) Cross-linked quaternary chitosan as an adsorbent for the removal of the reactive dye from aqueous solutions. J Hazard Mater 155:253–260
27. Atia AA, Donia AM, Al-Amrani WA (2009) Adsorption/desorption behavior of acid orange 10 on magnetic silica modified with amine groups. Chem Eng J 150:55–62
28. Extremera R et al (2012) Removal of acid orange 10 by calcined Mg/Al layered double hydroxides from water and recovery of the adsorbed dye. Chem Eng J 213:392–400
29. Uemura T et al (2008) Sol–gel synthesis of low-dimensional silica within coordination nanochannels. J Am Chem Soc 130:9216–9217